Structural and Functional Study of an Anemonia Elastase Inhibitor, a "Nonclassical" Kazal-Type Inhibitor from *Anemonia sulcata*‡

Hikaru Hemmi,[§,||] Takashi Kumazaki,[||,⊥,○] Kumiko Yoshizawa-Kumagaye,[@] Yuji Nishiuchi,[@] Takuya Yoshida,[#] Tadayasu Ohkubo,[#] and Yuji Kobayashi*[,#,◆]

National Food Research Institute, 2-1-12 Kannondai, Tsukuba, Ibaraki 305-8642, Japan, Faculty of Engineering, Aomori University, 2-3-1 Kobata, Aomori 030-0943, Japan, Peptide Institute Inc., Protein Research Foundation, Minoh, Osaka 562-8686, Japan, and Graduate School of Pharmaceutical Sciences, Osaka University, 1-6 Yamadaoka, Suita, Osaka 565-0871, Japan

Received December 28, 2004; Revised Manuscript Received April 15, 2005

ABSTRACT: *Anemonia* elastase inhibitor (AEI) is a "nonclassical" Kazal-type elastase inhibitor from *Anemonia sulcata*. Unlike many nonclassical inhibitors, AEI does not have a cystine-stabilized α-helical (CSH) motif in the sequence. We chemically synthesized AEI and determined its three-dimensional solution structure by two-dimensional NMR spectroscopy. The resulting structure of AEI was characterized by a central α-helix and a three-stranded antiparallel *β*-sheet of a typical Kazal-type inhibitor such as silver pheasant ovomucoid third domain (OMSVP3), even though the first and fifth half-cystine residues forming a disulfide bond in AEI are shifted both toward the C-terminus in comparison with those of OMSVP3. Synthesized AEI exhibited unexpected strong inhibition toward *Streptomyces griseus* protease B (SGPB). Our previous study [Hemmi, H., et al. (2003) *Biochemistry 42*, 2524−2534] demonstrated that the site-specific introduction of the engineered disulfide bond into the OMSVP3 molecule to form the CSH motif could produce an inhibitor with a narrower specificity. Thus, the CSH motif-containing derivative of AEI (AEI analogue) was chemically synthesized when a Cys^4−Cys^{34} bond was changed to a Cys^6−Cys^{31} bond. The AEI analogue scarcely inhibited porcine pancreatic elastase (PPE), even though it exhibited almost the same potent inhibitory activity toward SGPB. For the molecular scaffold, essentially no structural difference was detected between the two, but the N-terminal loop from Pro^5 to Ile^7 near the putative reactive site (Met^{10}-Gln^{11}) in the analogue moved by 3.7 Å toward the central helix to form the introduced Cys^6−Cys^{31} bond. Such a conformational change in the restricted region correlates with the specificity change of the inhibitor.

Anemonia elastase inhibitor (AEI) has been isolated from the whole body of the sea anemone *Anemonia sulcata* (*1*). AEI strongly inhibits porcine pancreatic elastase (PPE) and moderately inhibits human leukocyte elastase (HLE). No obvious inhibition has been observed toward trypsin, chymotrypsin (CHT), subtilisin, and cathepsin G. The biological role of this inhibitor has not been elucidated yet. AEI has three disulfide bridges in a molecule composed of 48 amino acid residues and is classified as part of the "nonclassical" Kazal-type inhibitor family based on the positioning of the first and fifth half-cystine residues forming the I−V disulfide bridge (*2*). The amino acid sequence of AEI is shown in Figure 1A, together with those of the classical and nonclassical Kazal-type inhibitors. Figure 2 shows the molecular structure of a representative classical Kazal-type inhibitor, OMSVP3 (*3*). It is apparent from the alignment of amino acid sequences of the nonclassical Kazal-type inhibitors that this type of inhibitor family could be further separated into two subgroups as will be described later.

One of the striking features of the nonclassical inhibitors would be that the first and fifth half-cystine residues forming the α′−*β*′ disulfide bond in wild-type AEI, crayfish inhibitor (*4*), and *Ciona* trypsin inhibitor (*5*) are all shifted toward the C-terminus in comparison with the respective half-cystine residues, I and V, for OMSVP3. We call these three inhibitors the "group 1" inhibitors, hereafter. Sequences of wild-type AEI, the AEI analogue, and OMSVP3 are specially extracted from Figure 1A to compare with them in detail (Figure 1B). AEI has three disulfide bridges, i.e., Cys^4−Cys^{34}, Cys^8−Cys^{27}, and Cys^{16}−Cys^{48}, where Cys^4 and Cys^{34} correspond to the first and fifth half-cystines in question, respectively, both of which are shifted by four residues toward the C-terminus compared with those for OMSVP3. It is rationalized on the basis of the sequence homology between AEI and OMSVP3 that the respective residues may

‡ The atomic coordinates for the 20 best conformers of wild-type AEI and AEI analogue described in this paper have been deposited with the Protein Data Bank (entries 1Y1B and 1Y1C, respectively). Chemical shifts for wild-type AEI and AEI analogue have been deposited in the BioMagResBank as entries 6386 and 6387, respectively.

* To whom correspondence should be addressed. E-mail: yujik@protein.osaka-u.ac.jp. Telephone: +81(6)68798220. Fax: +81(6)-68798221.

§ National Food Research Institute.

|| Both authors contributed equally to this work.

⊥ Aomori University.

@ Protein Research Foundation.

Osaka University.

○ Present address: Faculty of Pharmaceutical Sciences, Aomori University, 2-3-1 Kobata, Aomori 030-0943, Japan.

◆ Present address: Osaka University of Pharmaceutical Sciences, 4-20-1 Nasahara, Takatsuki, Osaka 569-1094, Japan.

10.1021/bi0472806 CCC: $30.25
Published on Web 06/22/2005

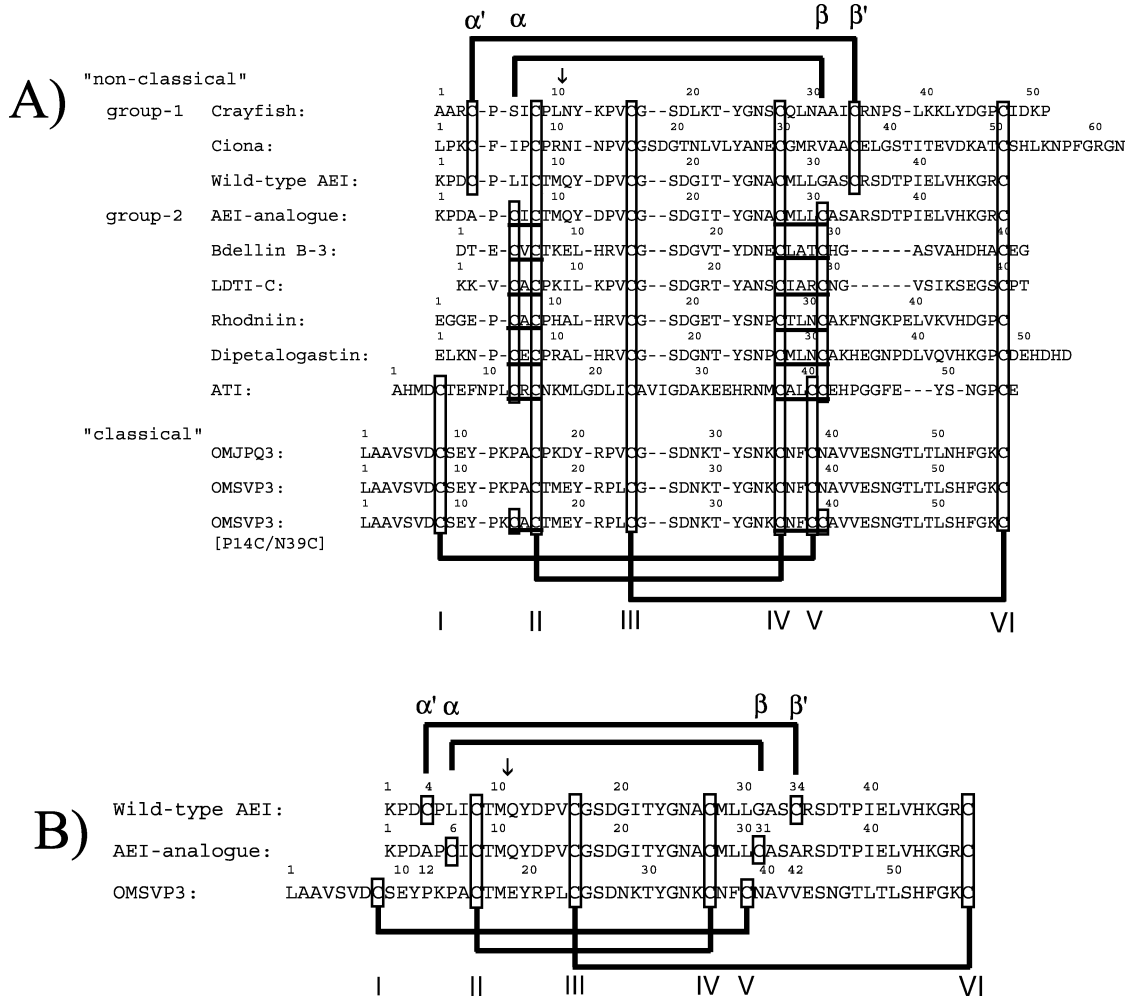

FIGURE 1: Alignment of amino acid sequences of AEI and some selective classical and nonclassical Kazal-type inhibitors (A). The sequences were aligned using CLUSTAL-W through Genome Net at the Institute for Chemical Research, Kyoto University, Kyoto, Japan. The reactive site is denoted with an arrow. Disulfide bonds are linked as follows: I−V, II−IV, and III−VI for the classical inhibitors, α′−β′, II−IV, and III−VI for the nonclassical group 1 inhibitors, and α−β, II−IV, and III−VI for the nonclassical group 2 inhibitors. ATI, which is classified as part of the nonclassical group 2 inhibitor family, has α−β in addition to I−V, II−IV, and III−VI. The sequence regions assigned to the CSH motif are underlined. According to Tamaoki et al. (*6*), the CSH motif in the group 2 inhibitors can be generally expressed as Cys-$(X)_m$-Cys/Cys-$(X)_n$-Cys, where $m/n = 1/3$. Contrary to this, the m/n value of the cystine pattern in the respective region of the group 1 inhibitors, including AEI, can be expressed as 3/6. References: AEI (*2*), crayfish inhibitor (Crayfish) (*4*), *Ciona* trypsin inhibitor (Ciona) (*5*), bdellin B-3 (*48*), LDTI-C (*14*), rhodniin (*13*), dipetalogastin (*49*), ATI (*15*), and OMJPQ3 and OMSVP3 (*17*). Panel B shows the sequence alignment of wild-type AEI, AEI analogue, and OMSVP3. Note that the three sequences can be aligned without introducing the gaps to improve the alignment.

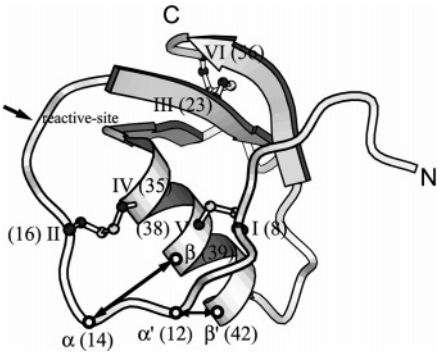

FIGURE 2: Molecular structure of OMSVP3 in a crystal state (*3*). The disulfide bonds (I−V, II−IV, and III−VI) and amino and carboxy termini (N and C, respectively) are also shown. Numbers in the parentheses are residue numbers of OMSVP3. Double-headed arrows point out two residues forming a disulfide bond in the nonclassical Kazal-type inhibitors.

correspond to positions α′ (residue 12) and β′ (residue 42) of OMSVP3 (also see Figure 2). The tertiary structures of the proteins with this type of disulfide pattern have not been elucidated yet.

Another feature is that five of eight nonclassical inhibitors have the cystine-stabilized α-helical (CSH)[1] motif in the sequence (see also Figure 1A), as already pointed out by Tamaoki et al. (*6*). We name these inhibitors the "group 2" inhibitors. In these cases, the first and fifth half-cystine

[1] Abbreviations: Boc, *tert*-butoxycarbonyl; Bom, benzyloxymethyl; CSH, cystine-stabilized α-helical; CZE, capillary zone electrophoresis; DQF-COSY, double-quantum-filtered correlation spectroscopy; ESI-MS, electrospray ionization mass spectrometry; HF, hydrogen fluoride; ^{1}H NMR, proton nuclear magnetic resonance; MCA, 4-methylcoumaryl-7-amide; native PAGE, polyacrylamide gel electrophoresis under nondenaturing conditions; NOE, nuclear Overhauser effect; NOESY, nuclear Overhauser effect spectroscopy; OMSVP3 and OMTKY3, ovomucoid third domains from silver pheasant and turkey, respectively; *p*NA, 4-nitroanilide; rmsd, root-mean-square deviation; RP-HPLC, reversed phase high-performance liquid chromatography; SGPA and SGPB, *Streptomyces griseus* proteases A and B, respectively; TFA, trifluoroacetic acid; TOCSY, total correlation spectroscopy; TPPI, time-proportional phase incrementation; 2D, two-dimensional.

residues forming the α−β disulfide bond are shifted by six and one residues, respectively, toward the C-terminus. The CSH motif is composed of an α-helical segment spanning the Cys-X_1-X_2-X_3-Cys portion that is cross-linked by two disulfide bridges to the Cys-X-Cys portion, folded in an extended β-strand-type structure. This motif has been widely found in bioactive peptides, such as endothelin-1, honeybee toxins (apamin), and scorpion toxins (charybdotoxin) (*7*−*9*). Each Cys-X_1-X_2-X_3-Cys segment was proven to form an α-helical structure by two-dimensional (2D) nuclear magnetic resonance (NMR) spectroscopy (*7*, *10*−*12*). Among the group 2 inhibitors, the tertiary structures of rhodniin-1 (*13*), LDTI-C (*14*), and ATI (*15*) have been determined, and each Cys-X_1-X_2-X_3-Cys segment was also proven to form a helical conformation.

In the course of study on elucidating the structural basis of the broad specificity of ovomucoid, we previously prepared the CSH motif-introducing variant of OMSVP3 with four disulfide bridges (P14C/N39C) on the basis of the sequence homology between OMSVP3 and ATI with four disulfide bridges (*16*). In the study, we obtained the unexpected results that P14C/N39C thus prepared lost almost all inhibitory activity toward PPE upon introduction of the Cys^{14}−Cys^{39} bond to form the CSH motif by cooperating with the preexisting Cys^{16}−Cys^{35} bond near the reactive site (see also Figure 2), although it retained the potent inhibitory activities toward CHT and *Streptomyces griseus* proteases A and B (SGPA and SGPB). Furthermore, structural studies have revealed that the preexisting α-helix structure is not broken, and that the conformational change of the reactive site loop from Cys^8 to Thr^{17} would affect the inhibitory specificity of this variant for the corresponding proteases. These results indicate that the site-specific introduction of the engineered disulfide bond near the reactive site proved to be useful in investigations of the relationship between the broad inhibitory specificity and the conformational flexibility of the Kazal-type inhibitors. It should be noted here that replacement of a Cys^4−Cys^{34} bond with a Cys^6−Cys^{31} bond in AEI would produce a CSH motif-containing group 2 inhibitor. The stereochemically possible model of AEI has been constructed (*2*), but the solution structure of AEI, in addition to those of the other two group 1 inhibitors, has not been analyzed yet. Structural and functional studies on wild-type AEI and the CSH motif-introducing AEI analogue would provide valuable information about the role of the unique α′−β′ disulfide bridge (see also panels A and B of Figure 1) in the structural stability and inhibitory specificity of the nonclassical Kazal-type inhibitors.

In this study, we first describe the synthesis and characterization of wild-type AEI and the CSH motif-containing AEI analogue. Second, the effects of introduction of the CSH motif on the inhibitory activities of AEI for different proteases are described. Third, determination of the solution structure of wild-type AEI and the AEI analogue by 2D NMR methods is described. Finally, we discuss the structural basis of the inhibitory specificity change of AEI caused by introduction of the CSH motif into the sequence near the reactive site.

EXPERIMENTAL PROCEDURES

Design of the AEI Analogue. In this study, naturally occurring AEI (wild-type AEI) and the CSH motif-containing derivative of AEI (AEI analogue) were chemically synthesized. AEI analogue thus designed is a Cys4Ala/Leu6Cys/Gly31Cys/Cys34Ala variant, which means that Cys is replaced with Ala at positions 4 and 34 and Leu and Gly at positions 6 and 31 are both replaced with Cys. Thus, the newly formed Cys^6−Cys^{31} bond should form the CSH motif into the AEI molecule by cooperating with the preexisting Cys^8−Cys^{27} bond. The numbering of ovomucoid third domains used in this study is that from Laskowski et al. (*17*).

Synthesis and Characterization. Wild-type AEI and AEI analogue were prepared by native chemical ligation (*18*) involving the coupling of (1−26)-thioester peptide and Cys^{27}-(28−48)-peptide. The synthesis of these peptide segments was performed with an ABI 433A peptide synthesizer (Applied Biosystems, Foster City, CA) using the Boc strategy. The purity of wild-type AEI and AEI analogue thus prepared was checked by reversed phase high-performance liquid chromatography (RP-HPLC) and capillary zone electrophoresis (CZE). Amino acid compositions of peptides and proteins were determined with an amino acid analyzer, and molecular weights of peptides were measured with electrospray ionization mass spectrometry (ESI MS). The complete synthetic methods and the peptide characterization described herein are found in the Supporting Information.

Location of the Disulfide Bridges. The native AEI protein (0.51 mg, 100 nmol) was digested with thermolysin (Daiwa Kasei, Osaka, Japan) (1/59 E/S, mol/mol) in 0.5 mL of 0.1 M ammonium acetate (pH 6.5) containing 1 mM $CaCl_2$, at 37 °C for 4 days. The digest was then subjected to a YMC-Pak ODS column (4.6 mm × 150 mm), and peptides were eluted using a 1 to 30% linear gradient of acetonitrile in 0.1% TFA for 50 min, monitoring the absorbance at 220 nm. Cystine-containing peptides were identified by comparing HPLC patterns of each digest before and after the treatment with dithiothreitol as a reducing reagent. The peptides thus identified were then characterized by ESI-MS and amino acid analysis to determine the disulfide linkages. For determination of the disulfide linkage in AEI analogue, almost the same procedure was applied, except that the AEI analogue protein was digested with thermolysin (1/30 E/S) for 11 days.

Enzyme Kinetics. PPE was kindly donated by Eisai Co. (Tokyo, Japan). SGPB was prepared as described by Narahashi (*19*). Wild-type OMSVP3 was prepared as described previously (*16*). The following enzymes and substrates were purchased from Sigma Chemical Co. (St. Louis, MO): CHT, HLE, $α_1$-antitrypsin, bovine trypsin, *p*-nitrophenyl *p*′-guanidinobenzoate, Suc-Ala-Ala-Ala-*p*NA, Suc-Ala-Ala-Val-*p*NA, Suc-Ala-Ala-Pro-Phe-*p*NA, and Suc-Ala-Ala-Pro-Phe-MCA. All assays were carried out at 25 °C in 50 mM Tris-HCl (pH 7.8) containing 20 mM $CaCl_2$ and 0.005% Triton X-100. The active site concentration of CHT was first determined, as described by Bender et al. (*20*). Wild-type OMSVP3 was then titrated with a known concentration of CHT, as previously reported (*16*). The active site concentrations of SGPB and PPE were finally determined by titrating with a known concentration of OMSVP3. For determination of the active site concentration of HLE, the concentration of trypsin was first determined using a specific titrant for trypsin, *p*-nitrophenyl *p*′-guanidinobenzoate (*21*). $α_1$-Antitrypsin was then titrated with a known concentration of trypsin. Finally, the concentration of HLE was determined by titrating with a known concentration of $α_1$-antitrypsin. For assays of PPE

and HLE, Suc-Ala-Ala-Ala-*p*NA and Suc-Ala-Ala-Val-*p*NA were used as substrates, respectively. Suc-Ala-Ala-Pro-Phe-*p*NA and Suc-Ala-Ala-Pro-Phe-MCA were used for the assay of SGPB. For measurement of association rate constants (k_{on} values), the enzyme solution was added to a mixture of inhibitor and substrate. The progress curve corresponding to the pre-steady state was traced on a Hitachi U-2010 spectrophotometer or on a Hitachi F-2500 fluorescence spectrophotometer for up to ~10 min, and the data thus obtained were analyzed according to the method of Bieth (*22*). The inhibitor concentration was chosen so that $[I]_0 \geq 5[E]_0$, and a substrate concentration of less than $0.3K_m$ was also chosen. The equilibrium dissociation constants (K_i values) were determined essentially as previously described (*16*). In brief, mixtures of an enzyme with various concentrations of an inhibitor were incubated for a time sufficient to establish equilibrium (0.5−6.0 h). Enzyme concentrations were as follows: 1.0 nM PPE for the wild-type AEI−PPE interaction, 60 nM PPE for the AEI−analogue−PPE interaction, 60 nM HLE for the AEI−HLE interaction, and 0.30 nM SGPB for the AEI−SGPB interaction. To each equilibrium mixture was added a small volume of a suitable *p*NA substrate described above, and the residual enzyme activity was measured. Then, the fractional residual activity was plotted against the inhibitor concentration. The K_i values were estimated by nonlinear regression analysis according to Bieth (*22*). Data fitting to obtain the parameters such as the K_i and k_{on} values was carried out using KaleidaGraph for Windows (Synergy Software).

NMR Experiment. The AEI samples were dissolved in 500 μL of 100% D_2O or a 90% H_2O/10% D_2O solution to give a final concentration of approximately 3 mM. The pH of the solution was adjusted to 2.4. All NMR spectra were obtained on Bruker Avance500, DRX600, and Avance800 spectrometers with quadrature detection in the phase-sensitive mode by TPPI (*23*) and States−TPPI (*24*) methods. The following spectra were recorded at 20, 25, 30, 35, and 40 °C with 15 ppm spectral widths in the t_1 and t_2 dimensions: 2D double-quantum-filtered correlated spectroscopy (DQF-COSY) (*25*), recorded with 512 and 2048 complex points in the t_1 and t_2 dimensions, respectively; 2D homonuclear total correlated spectroscopy (TOCSY) (*26*) with a DIPSI-2 mixing sequence, recorded with mixing times of 35, 60, and 80 ms, with 512 and 2048 complex points in the t_1 and t_2 dimensions, respectively; 2D nuclear Overhauser effect spectroscopy (NOESY) (*27*), recorded with mixing times of 60, 100, and 200 ms, with 512 and 2048 complex points in the t_1 and t_2 dimensions, respectively; and 2D rotating frame nuclear Overhauser effect spectroscopy (ROESY) (*28*), recorded with a mixing time of 100 ms, with 512 and 2048 complex points in the t_1 and t_2 dimensions, respectively. The high-digital resolution DQF-COSY and exclusive 2D scalar COSY (E-COSY) (*29*) spectra were recorded using 400 and 4096 complex points in the t_1 and t_2 dimensions, respectively. Water suppression was performed using the WATERGATE sequence (*30*, *31*). Two-dimensional $^1H-^{15}N$ heteronuclear single-quantum correlation spectroscopy (HSQC) (*32*) was carried out with 1024 × 128 complex points for 15 ppm in the ^1H dimension and 40 ppm in the ^{15}N dimension at 25, 40, and 50 °C, and 256 or 512 transients at natural abundance. Slowly exchanging amide protons were identified by lyophilizing the protein from a H_2O solution, dissolving the protein in D_2O, and collecting sequential 2 h 2D TOCSY spectra. All NMR spectra were processed using XWINNMR (Bruker Instruments). Before Fourier transformation, the shifted sine-bell window function was applied to the t_1 and t_2 dimensions. Peak picking and assignment were performed with Sparky (T. D. Goddard and D. G. Kneller, *SPARKY 3*, University of California, San Francisco). Chemical shifts were referenced to internal 2,2-dimethyl-2-silapentane-5-sulfonate (DSS) at 25 °C.

Structure Calculations. NOE-derived distance restraints were classified into three ranges (1.8−2.5, 1.8−3.5, and 1.8−5.0 Å), according to the relative NOE intensities. Upper distance limits for NOEs involving methyl protons and nonstereospecifically assigned methylene protons were corrected appropriately for center averaging (*33*). In addition, a distance of 0.5 Å was added for the upper distance limits for only NOEs involving methyl protons (*34*) after the correction for center averaging. Torsion angle constraints on backbone ϕ and ψ angles were derived from $^3J_{HN\alpha}$ coupling constants estimated from the high-digital resolution 2D DQF-COSY spectra, and sequential and short-range NOEs. The 27 and 31 ϕ angle restraints were obtained for wild-type AEI and AEI analogue, respectively. Backbone ϕ angles were restrained to $-60 \pm 30°$ when $^3J_{N\alpha} < 6$ Hz, $-120 \pm 50°$ when $^3J_{N\alpha} = 8-9$ Hz, and $-120 \pm 40°$ when $^3J_{N\alpha} > 9$ Hz. A ψ angle restraint was used for residues in α-helix and β-strand structures, as predicted from NOE patterns characteristic of secondary structure and the preliminary structures. Eleven ψ angle restraints were obtained for both wild-type AEI and AEI analogue. The ψ angle was restrained to $-40 \pm 30°$ in the α-helix regions and $120 \pm 60°$ in the β-sheet regions. Side chain χ_1 angles were determined by $^3J_{H\alpha H\beta}$ coupling constants from exclusive 2D scalar COSY and short mixing TOCSY connectivities in combination with NH−Hβ and Hα−Hβ NOEs (*35*). The 10 and 12 χ_1 angle restraints for the wild type and AEI analogue, respectively, were obtained. The χ_1 angle restraints were normally restricted to a ±60° range from staggered conformations, g+ (60°), t (180°), or g− (−60°). Hydrogen−deuterium exchange experiments identified 46 hydrogen bond donors for wild-type AEI and AEI analogue. Corresponding hydrogen bond acceptors were determined on the basis of NOE patterns observed for regular secondary structural regions and preliminary calculated structures without restraints regarding hydrogen bonds. Hydrogen bond constraints were applied to N−H and C═O groups: 1.7−2.4 Å for the H−O distance and 2.7−3.4 Å for the N−O distance. The chemically determined disulfide connectivities for AEI or AEI analogue were included at the beginning of the structure calculation. Covalent bonds between the sulfur atoms of disulfide bridges were handled as fake NOE distances according to the standard X-PLOR protocol (*36*).

Structure calculations were performed using ab initio simulated annealing from an extended template in X-PLOR, version 3.851 (*36*). A set of 672 NOE-derived distance restraints (including 94 intraresidue, 229 sequential, 124 medium-range, and 225 long-range), 46 hydrogen bond restraints, and 48 dihedral angle restraints were obtained for wild-type AEI. In case of AEI analogue, a set of 664 NOE-derived distance restraints (including 98 intraresidue, 225 sequential, 134 medium-range, and 207 long-range), 46 hydrogen bond restraints, and 54 dihedral angle restraints

were obtained. The structure calculation proceeded in two stages by using the standard X-PLOR protocol. In the first stage, a low-resolution structure was preliminarily determined using NOE-derived distance restraints and dihedral angle restraints except for ψ angle restraints. In the second stage of the calculation, the same protocol was applied by adding hydrogen bond restraints and ψ angle restraints. The force constants for the distance restraints were set to 50 kcal mol^{-1} $Å^{-2}$ throughout all the calculations, and dihedral angle restraints were initially set to 5 kcal mol^{-1} rad^{-2} during the high-temperature dynamics and gradually increased to 200 kcal mol^{-1} rad^{-2} during the annealing stage. The final round of calculations began with 200 initial structures, 56 for wild-type AEI and 70 for AEI analogue of which, after refinement, had no distance and dihedral angle violations greater than 0.5 Å and 5°, respectively. Among the 56 and 70 final structures, the 20 structures of wild-type and AEI analogue with low total energy and low deviation from mean structure were used for further analyses. The average coordinates of the ensembles of the 20 low-energy structures of wild-type AEI or AEI analogue were subjected to 500 or 1000 cycles of Powell restrained minimization, respectively, to improve stereochemistry and nonbonded contacts. All subsequent numerical analyses were performed using X-PLOR, PROCHECK-NMR (*37*), and MOLMOL (*38*). Structure figures were generated using Molscript (*39*) and MOLMOL.

Molecular Modeling of the Hypothetical Complexes between Wild-Type AEI (or AEI Analogue) and Serine Proteases. The complex model between AEI and HLE (or SGPB) was constructed by superimposing the reactive site region from P_3 to P_2' between AEI and OMTKY3 in the HLE−OMTKY3 complex (or in the SGPB−OMTKY3 complex) and by exchanging the two inhibitors using the method of Read and James (*40*). The complex model between AEI analogue and HLE (or SGPB) was also constructed similarly. On the other hand, the complex model between AEI and PPE was constructed by superimposing the coordinates for PPE onto those of HLE in the HLE−AEI complexes obtained above, and by exchanging the two elastases using the method of Baker and Murphy (*41*). The coordinates used in this study are as follows: PDB entry 1PPF for the HLE−OMTKY3 complex, PDB entry 3SGB for the SGPB−OMTKY3 complex, and PDB entry 3EST for PPE.

RESULTS

Synthesis and Characterization. To analyze the tertiary structure of AEI, we synthesized a 48-amino acid residue protein with three disulfide bridges. Furthermore, we tried to synthesize AEI analogue with the CSH motif by replacement of a Cys^4−Cys^{34} bond with a Cys^6−Cys^{31} bond to address the structural basis of the restricted specificity of AEI. AEI and its analogue were successfully prepared by native chemical ligation involving the coupling of (1−26)-thioester peptides and Cys^{27}-(28−48)-peptides. These peptide segments were elongated by the standard solid phase peptide synthesis with the Boc chemistry followed by deprotection using HF. The advantage of the Boc chemistry is that it can avoid the side reactions such as epimerization of the C-terminal Cys residue (*42*) and/or aspartimide formation of Asp-X sequences (*43*). Under the standard HF reaction conditions, however, (27−48)-peptide having the N-terminal Cys residue was accompanied by the side reaction, i.e., thioproline formation, associated with use of the Bom group for the His residue. The addition of cysteine hydrochloride proved to be effective for suppressing this side reaction as reported previously (*44*, *45*). The reduced form of AEI was successfully folded at pH 7.8 in the presence of reduced and oxidized glutathione. The principal products of wild-type AEI and its analogue were isolated in 71 and 74% yield, respectively, calculated from their reduced peptides. The purity of wild-type AEI and AEI analogue thus prepared was verified to be more than 97% by both RP-HPLC and CZE. The homogeneity was also verified on native PAGE. Amino acid compositions and the molecular weights of these proteins were both in good agreement with the respective theoretical values (Table S1 of the Supporting Information).

Location of the Disulfide Bridges. To determine the disulfide structure of AEI and its analogue, these two proteins were digested with thermolysin to isolate the cystine-containing peptides. The peptides thus obtained from each digest were assigned by ESI-MS and amino acid analysis. The results are shown in Table S1 of the Supporting Information, supporting the fact that the combinations of the disulfide bonds in synthetic AEI were the same as those reported for natural AEI, i.e., Cys^4−Cys^{34}, Cys^8−Cys^{27}, and Cys^{16}−Cys^{48} (*2*). As for AEI analogue, obtained data also support the same disulfide bridging pattern as that of the natural one, i.e., Cys^6−Cys^{31}, Cys^8−Cys^{27}, and Cys^{16}−Cys^{48}.

Inhibitory Specificities of AEI and AEI Analogue. It has been reported that naturally occurring AEI can strongly inhibit PPE and moderately inhibit HLE (*1*), and that the inhibitor cannot obviously inhibit trypsin, CHT, subtilisin, and cathepsin G. Considering that OMSVP3 having the P_1 Met residue can inhibit different proteases, i.e., CHT, SGPA, SGPB, subtilisin BPN′, PPE, and HLE, with various substrate specificities (*46*), it is reasonably expected that AEI with the same P_1 Met residue may inhibit some serine proteases other than elastase. Thus, we tried to test the inhibitory activity of AEI toward SGPB, as well as those for PPE and HLE. The kinetic parameters (K_i and k_{on} values) of the interaction between AEI and the three different proteases, together with those for AEI analogue, were determined (Table 1). The K_i values for synthesized AEI were essentially the same as those reported for natural AEI (*1*), indicating that synthesized AEI is functionally equivalent to the natural form. Further, AEI was found to exhibit the unexpected strong inhibition toward SGPB. For the association rate constants (k_{on}), AEI gave high values ($>10^6$ M^{-1} s^{-1}) for PPE and SGPB. These new results suggest that AEI may not be called an "elastase-specific" inhibitor in a strict sense.

The kinetic parameters of the interaction between the three different proteases for AEI analogue are also shown in Table 1. The striking features of this table would be that AEI analogue exhibits a dramatic decrease in inhibition toward PPE by a factor of 10^5 in comparison with wild-type AEI, while AEI analogue retained almost the same inhibitory activities toward HLE and SGPB as wild-type AEI. AEI analogue gave almost the same k_{on} value for SGPB as wild-type AEI. We were unable to measure the k_{on} value of AEI analogue for PPE, since the pre-steady exponential phase exhibiting the binding between enzyme and inhibitor could not be observed on the conventional apparatus used in this study. The dissociation constant is equivalent to k_{off}/k_{on}, and

Table 1: Kinetic Parameters for Wild-Type AEI and AEI Analogue against Serine Proteases[a]

	PPE		HLE		SGPB	
	K_i (M)	k_{on} (M^{-1} s^{-1})	K_i (M)	k_{on} (M^{-1} s^{-1})	K_i (M)	k_{on} (M^{-1} s^{-1})
natural AEI	$\sim 10^{-10}$ [b]	ND[c]	$\sim 10^{-7}$ [b]	ND[c]	ND[c]	ND[c]
wild-type AEI	7.0×10^{-11}	2.4×10^{6}	1.4×10^{-7}	ND[c]	1.7×10^{-11}	6.1×10^{6}
AEI analogue	9.0×10^{-6}	$\sim 2 \times 10$[d]	3.6×10^{-8}	ND[c]	3.6×10^{-12}	3.7×10^{6}

[a] The kinetic parameter values are usually determined from two experiments, so standard deviation (SD) values are not given. Correlation coefficients are all more than 0.998, which shows that the data points are fit with low error to the theoretical equation according to the method of Bieth (*22*). [b] Data from ref *1*. [c] Not determined. [d] Estimated on the assumption that the k_{off} value (2×10^{-4} s^{-1}) calculated for the wild-type AEI−PPE interaction is applicable for the AEI analogue−PPE interaction.

so the dramatic decrease in K_i for the AEI analogue−PPE interaction could be explained either by a dramatic decrease in k_{on} or by a dramatic increase in k_{off}. If the calculated k_{off} value (2×10^{-4} s^{-1}) for the AEI−PPE interaction is applicable for the AEI analogue−PPE interaction, a very low k_{on} value ($\sim 2 \times 10$ M^{-1} s^{-1}) could be estimated. Thus, AEI analogue cannot practically associate with PPE. We have observed an analogous result of specificity change upon introduction of the CSH motif into the OMSVP3 molecule (*16*). The resistance of natural AEI to enzymatic degradation by PPE has been observed by prolonged exposure to this enzyme at pH values from 3 to 8 (*1*). Here, we examined the susceptibility of AEI to elastase digestion under the assay conditions by native PAGE analysis. The results indicated that AEI analogue, as well as wild-type AEI, was hardly degraded even after a 24 h incubation with PPE (1/8 E/S, mol/mol) at pH 7.8 and 25 °C (data not shown). Thus, this dramatic decrease in inhibitory activity of AEI analogue toward PPE would be due to the lack of tight binding to enzyme, but not due to enzymatic degradation of this analogue.

Resonance Assignments and Secondary Structure. The sequence-specific assignments of the proton resonance from the residue in wild-type AEI, as well as AEI analogue, were determined using standard procedures (*47*) from 2D NMR spectra collected at 20, 25, 30, 35, and 40 °C. For assignments of Pro residues, Hα(*i*)−Hδ(*i*+1:Pro) (dα*δ*) or Hα(*i*)−Hα(*i*+1:Pro) (dαα) NOEs were used instead of dαN. In the previous study (*16*), we found that the Tyr^{11}-Pro^{12} *cis*-peptide linkage in OMSVP3, which is highly conserved in ovomucoid third domains, is isomerized to the trans configuration upon introduction of an engineered Cys^{14}−Cys^{39} bond into the molecule. Therefore, we paid a special attention to the configuration of the Cys^{4}−Pro^{5} bond in AEI and the Ala^{4}−Pro^{5} bond in AEI analogue corresponding to the Tyr^{11}−Pro^{12} bond in OMSVP3. The proline residues at positions 2, 5, 14, and 39 in both inhibitors gave all strong dα*δ* NOEs, indicating that all the proline residues of the two proteins have a trans configuration. The proton peak assignments of AEI, as well as AEI analogue, in the 2D NMR spectra were completed. The resonance assignments were extended by determining stereospecific assignments of some methylene protons to obtain high-precision NMR structures. Stereospecific assignments of *β*-methylene protons were obtained for 10 of 28 residues of wild-type AEI (for 12 of 27 residues of AEI analogue). To investigate structural differences between wild-type AEI and AEI analogue, the ^{1}H chemical shifts of NH and CαH groups were compared (Figure 3). Significant differences (>0.2 ppm) are detected for residues, Ile^{7}, Cys^{8}, and Met^{10}, in addition to the substituted amino acid residues at positions 4, 6, 31, and 34. The two proteins assume different conformations for the N-terminal region constituting residues from position 6 to 8 but almost the same structures for the remaining C-terminal region. This idea is supported by the observation that AEI, as well as AEI analogue, contains the secondary structure elements, an α-helix (Ala^{26}−Arg^{35}) and a three-stranded antiparallel *β*-sheet (Val^{15}−Ser^{18}, Ile^{21}−Tyr^{23}, and Glu^{41}−His^{44}), deduced from NOE patterns, $^3J_{HNH\alpha}$ coupling constants, and amide proton exchange data (Figure S1 of the Supporting Information).

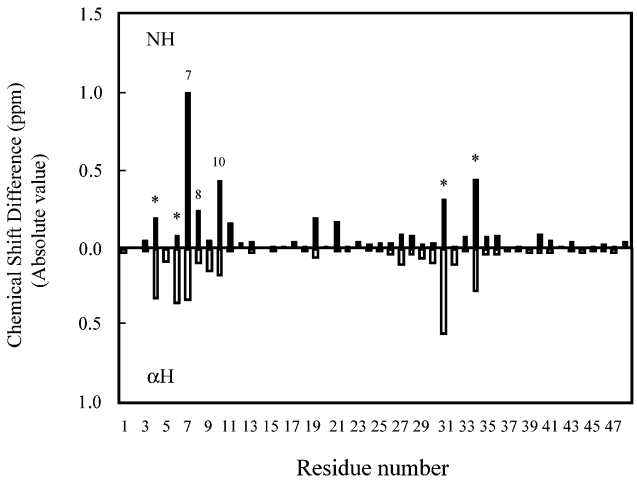

FIGURE 3: ^{1}H chemical shift difference of CαH and NH between wild-type AEI and AEI analogue. The asterisk indicates substituted amino acid residues, from Leu or Gly to Cys and from Cys to Ala.

Tertiary Structure. The three-dimensional structure of wild-type AEI, as well as that of AEI analogue, was determined by an ab initio simulated annealing approach based upon 766 (764 for AEI analogue) experimental restraints derived from NMR data. Structural statistics for the final 20 structures and the restrained energy-minimized average structure are given in Table 2. Panels A and C of Figure 4 show the best-fit superpositions of backbone atoms of the 20 structures for wild-type AEI and AEI analogue, respectively. Ribbon diagrams of the corresponding restrained energy-minimized average structures are shown in panels B and D of Figure 4. The rmsd values for backbone atoms relative to the mean structure in the region from Cys^{8} to Cys^{48} were 0.549 Å for wild-type AEI and 0.468 Å for AEI analogue. These data indicate that most of the whole molecule for both proteins converges very well in the calculated structures. Their solution structures are both comprised of a three-stranded antiparallel *β*-sheet (strand 1, Val^{15}−Ser^{18}; strand 2, Ile^{21}−Tyr^{23}; and strand 3, Glu^{41}−His^{44}) and a central α-helix (Ala^{26}−Arg^{35}), demonstrating that this protein has the characteristic scaffold of a typical classical

Table 2: Structural Statistics[a]

	wild-type AEI		AEI analogue	
	⟨SA⟩	⟨SA⟩r	⟨SA⟩	⟨SA⟩r
total no. of distance restraints	718		710	
intraresidue	94		98	
sequential	229		225	
medium-range ($1 < \|i - j\| < 5$)	124		134	
long-range ($\|i - j\| \geq 5$)	225		207	
hydrogen bond (two per bond)	46		46	
total no. of dihedral angle restraints	48		54	
ϕ	27		31	
ψ	11		11	
χ_1	10		12	
rms deviations from experimental restraints				
distance restraints (Å)	0.032 ± 0.0018	0.032	0.034 ± 0.0008	0.035
dihedral angles (deg)	0.674 ± 0.112	0.699	0.678 ± 0.090	0.614
rms deviations from idealized geometry				
bonds (Å)	0.003 ± 0.0001	0.003	0.003 ± 0.0001	0.003
angles (deg)	0.516 ± 0.020	0.518	0.529 ± 0.011	0.519
impropers (deg)	0.374 ± 0.025	0.364	0.445 ± 0.019	0.412
energies (kcal/mol)				
total	114.2 ± 7.77	114.7	127.2 ± 3.12	127.5
bond	8.45 ± 0.82	8.17	9.44 ± 0.58	9.61
angle	51.9 ± 4.31	52.2	54.1 ± 2.3	52.1
impropers	7.41 ± 0.99	6.98	10.43 ± 0.90	8.90
van der Waals[b]	8.23 ± 2.45	9.03	10.34 ± 1.64	10.80
dihedral[c]	1.87 ± 0.46	1.43	1.54 ± 0.41	1.24
NOE[c]	36.8 ± 4.3	36.8	41.3 ± 2.1	44.8
ϕ and ψ in core and allowed regions (%)[d]	99.3	100	100	100
rmsd relative to the mean structure (Å)				
residues 8−48 for the backbone	0.549 ± 0.174		0.468 ± 0.106	
residues 8−48 for all non-H	1.175 ± 0.238		0.919 ± 0.087	

[a] ⟨SA⟩ represents the 20 and 20 individual structures for wild-type AEI and AEI analogue, respectively, calculated with the X-PLOR program (*36*). ⟨SA⟩r is the refined structure obtained by energy minimization of the mean structure obtained by simple averaging of the coordinates of the SA structures. [b] The van der Waals energy was calculated using a final value of 4 kcal mol^{-1} Å^{-2} with the van der Waals hard sphere radii set to 0.75 times the standard values used in the CHARMM empirical energy function. [c] Dihedral and NOE energies were calculated using force constants of 200 kcal mol^{-1} rad^{-2} and 50 kcal mol^{-1} Å^{-2}, respectively. [d] PROCHECK-NMR (*37*) was used to assess the stereochemical parameters of the family of conformers.

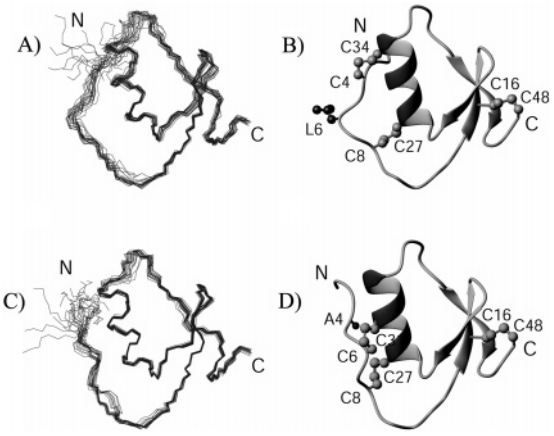

FIGURE 4: Superimposition of the best 20 structures of AEI (A) or AEI analogue (C) and ribbon diagrams of the minimized average structures of wild-type AEI (B) or AEI analogue (D). The disulfide bridges (Cys^4−Cys^{34}, Cys^6−Cys^{31}, Cys^8−Cys^{27}, and Cys^{16}−Cys^{48}), the side chain of Ala^4, and the side chains of Leu^6 are ball-and-stick representations. This figure was generated using MOLMOL (*38*).

Kazal-type inhibitor, such as OMSVP3 (*3*). The inhibitor molecule of AEI has been modeled on the basis of the known tertiary structure of OMSVP3 (*2*). If the remarkable similarity of tertiary structures between AEI and OMSVP3 is taken into consideration, it would be reasonable that a stereochemically possible model of AEI could have been constructed without strain and significant rearrangement (*2*). The two proteins, AEI and AEI analogue, showed significant structural difference in the N-terminal parts. We will give details of this matter later.

Structural Comparison between Wild-Type AEI and AEI Analogue. We have mentioned that the solution structure of AEI analogue is very similar to that of wild-type AEI, which is comprised of a three-stranded antiparallel β-sheet (strand 1, Val^{15}−Ser^{18}; strand 2, Ile^{21}−Tyr^{23}; and strand 3, Glu^{41}−His^{44}) and a central α-helix (Ala^{26}−Arg^{35}). The preexisting α-helix structure in AEI is not broken upon changing the Cys^4−Cys^{34} bond to the non-natural Cys^6−Cys^{31} bond. The overall structures of wild-type AEI and AEI analogue are quite similar to each other (see also Figure 4). Particularly, the backbones of the well-defined C-terminal parts from residue 12 to 48 of the two proteins are superimposable, as shown in Figure 5A. Residual backbone rmsd values for the C-terminal parts are less than 1.2 Å for both proteins (see Figure S2 of the Supporting Information). Those values for the N-terminal parts consisting of residues 5−7 are larger than 2 Å (where N-terminal three residues are omitted for calculation) (see also Figure S2 of the Supporting Information). These results are in good agreement with the ^{1}H chemical shift differences of NH and CαH groups between the two proteins (see also Figure 3). The most significant deviation is observed within the N-terminal loop from Pro^5 to Ile^7. It turned out that this loop is drawn closer to the

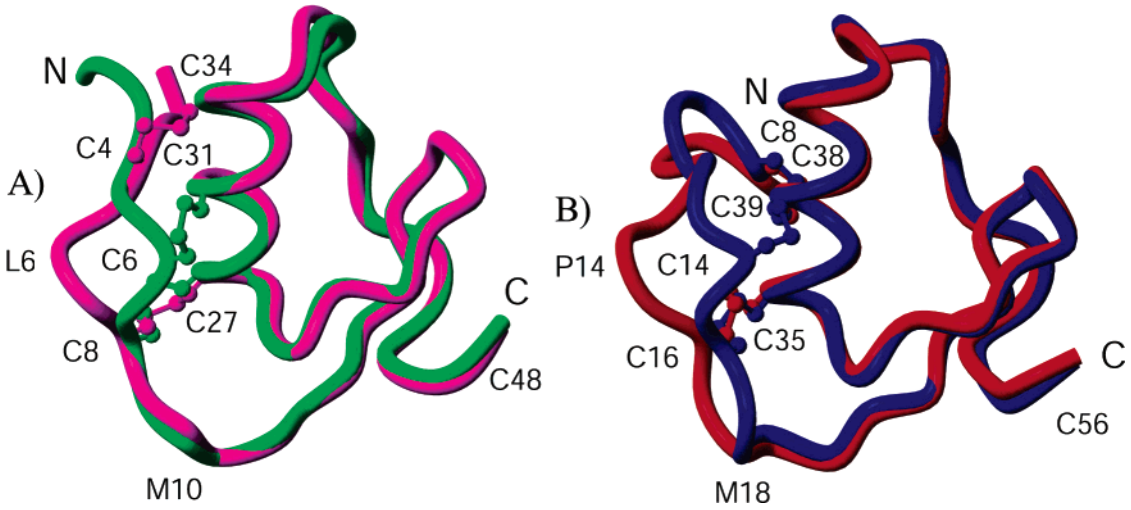

FIGURE 5: Schematic representation of main chain folding of wild-type AEI (magenta) overlaid with that of AEI analogue (green) (A) and that of OMSVP3 (red) overlaid with that of P14C/N39C (blue) with the CSH motif (*16*). Note that the six N-terminal residues of OMSVP3 and P14C/N39C (B) have been omitted from the models. Disulfide bonds (Cys^4-Cys^{34}, Cys^6-Cys^{31}, Cys^8-Cys^{27}, etc.) are ball-and-stick representations. Some residues described in the text are also represented. These figures were generated by MOLMOL (*38*).

central helix by approximately 3.7 Å, since the Cα−Cα distance between Leu^6 and Gly^{31} is 8.4 Å in wild-type AEI, whereas the respective distance is 4.7 Å after the formation of the Cys^6-Cys^{31} bond. The large ^1H chemical shift differences detected for the N-terminal region described above may reflect a conformational change except for Met^{10} (see also Figure 3). A significant difference for the ^1H chemical shift of NH of Met^{10} is observed even though the conformation around Met^{10} is very similar between the two. In $^{15}N-^1H$ HSQC spectra, the resonance signal of Met^{10} in AEI analogue was observed at 25 °C, but that in AEI was missing at 25 and/or 40 °C and observed at 50 °C. These results suggest that the significant ^1H chemical shift difference of the NH group of Met^{10} may be due to the conformational flexibility around Met^{10}. Our structural data indicate that the hydrophobic side chain of Leu^6 in AEI faces the solvent. Thus, the disulfide bond formation between positions 6 and 31 should lead to considerable conformational changes in the loop from residue 6 to 8, accompanied by side chain rotation and main chain movement. It is worth emphasizing that replacement of a Cys^4-Cys^{34} bond with a Cys^6-Cys^{31} bond has little effect on the C-terminal part, particularly on the central helix, because it is designed to provide the CSH motif to the AEI molecule by cooperating with the preexisting Cys^8-Cys^{27} bond. Structural basis of the inhibitory specificity change due to introduction of the CSH motif will be described in Discussion.

DISCUSSION

AEI from *A. sulcata* is classified into the nonclassical Kazal-type inhibitor family (*2*). Eight nonclassical Kazal-type inhibitors have been isolated from various animals and characterized so far (*4*, *5*, *13*−*15*, *48*, *49*). In this study, we have first demonstrated that these nonclassical inhibitors could be further separated into the subgroups, such as group 1 and group 2 according to the rule of positioning of the first and fifth half-cystine residues forming the disulfide bond. The tertiary structures of rhodniin-1, LDTI-C, and ATI of group 2 have been determined, and each Cys-X_1-X_2-X_3-Cys segment of the CSH motif was proven to form a helical conformation. Contrary to this, the solution structure of AEI of group 1, in addition to those of the other two, has not been analyzed yet. To address the structural basis of the restricted specificity of AEI, we synthesized AEI, a 48-amino acid residue protein with three disulfide bridges. Further, the CSH motif-containing AEI analogue was prepared similarly by replacing the Cys^4-Cys^{34} bond with the non-natural Cys^6-Cys^{31} bond. The two proteins were successfully prepared by native chemical ligation. Many examples of the chemical syntheses of protease inhibitors, i.e., elafin (*50*), BPTI (*51*), and hirudin (*52*), have been reported. Results obtained in this study were quite satisfactory for, in particular, the purity, the folding efficiencies, and the correct folding.

Synthesized AEI exhibited strong inhibition toward PPE, as expected for the natural inhibitor. In addition, AEI exhibited the unexpected strong inhibition toward SGPB. On the other hand, AEI analogue scarcely inhibits PPE, while it retained potent inhibitory activity toward SGPB. The CSH motif-introducing Kazal-type inhibitors, such as AEI analogue and P14C/N39C, lost almost all inhibitory activity toward PPE. These results suggest that an increase in rigidity near the reactive site may produce an inhibitor with a narrower specificity. It is worth noting that these CSH motif-introducing inhibitors are not cleaved by PPE, because they cannot bind to the proteases. This is in marked contrast to the inhibitors that show no inhibition when their target enzymes are often cleaved by these enzymes (*53*, *54*). The solution structure of AEI, as well as AEI analogue, was determined using 2D NMR methods. The resulting structure of AEI has a common characteristic scaffold composed of a three-stranded antiparallel β-sheet and a central α-helix like the solution and crystal structures of OMSVP3 (see Figure 5). In the classical Kazal-type inhibitor with three disulfide bridges, the N-terminal loop is anchored to the central helix via two disulfide bridges, I−V and II−IV, which stabilize the reactive site loop. In the case of AEI, the two disulfide bridges, such as the Cys^4-Cys^{34} and Cys^8-Cys^{27} bridges, could be used for this purpose, where the former corresponds to a disulfide bond between residues 12 and 42 of OMSVP3 (see Figure 1B) and the latter to the highly conserved Cys^{16}−

Cys^{35} bond near the reactive site $Met^{18}-Glu^{19}$ peptide bond. Why is the I−V disulfide bridge in the nonclassical Kazal-type inhibitors placed near the conserved II−IV disulfide bond? This would be partly explained by the fact that the N-terminal loop of the nonclassical inhibitors is shorter than that of the classical ones. In the case of AEI, the first and fifth half-cystine residues are shifted both by four residues to the C-terminus (see also Figure 1B), which makes it possible to allow a proper formation of a I−V disulfide bond. The CSH motif-containing inhibitors, including AEI analogue, would make use of a disulfide bond between residues 14 and 39 and the conserved $Cys^{16}-Cys^{35}$ bond of OMSVP3 for the same purpose. It is apparent that bdellin B-3 and LDTI-C, with the extremely shortened N-terminal loop, could not anchor the loop to the central helix using the disulfide bridge at the same position compared with that of the classical inhibitor. In these inhibitors, the CSH motif would be used for anchoring the loop. In cases of AEI, crayfish inhibitor, and *Ciona* trypsin inhibitor, the shortened N-terminal loop would be fixed by a disulfide bond shifted by one turn in the helix. An exceptional example for anchoring of the N-terminal loop to the central helix is shown in ATI with four disulfide bridges, where the three half-cystine residues corresponding to Cys^8, Cys^{14}, and Cys^{16} of OMSVP3 are used for this purpose. Structural comparison of AEI with AEI analogue will be discussed below in addressing the structural basis of the inhibitory specificity change due to introduction of the CSH motif.

Structural Basis of the Inhibitory Specificity Change Due to Introduction of the CSH Motif. It is generally accepted that the P_1 site residue of serine protease inhibitors is a predominant determinant of inhibitory specificity (*53*, *55*−*59*). Comparative studies using more than 100 species of the third domains of ovomucoids demonstrated that changes in residues other than the P_1 site residue can often exert large differential effects toward the different enzymes (*2*). Comparison of the solution structures of wild-type AEI and AEI analogue revealed that significant differences were detected for the loop region from Pro^5 to Ile^7. The loop moves by 3.7 Å to the central helix due to formation of the Cys^6-Cys^{31} bond. In our previous paper (*16*), the structural data which show that the loop region from Cys^8 to Thr^{17} of P14C/N39C moves by 4 Å toward the central helix compared with that of wild-type OMSVP3 (see also Figure 5B), together with the functional data for other OMSVP3 variants, suggested that the main cause of the inhibitory specificity change would be the conformational change of the reactive site loop due to disulfide bond formation. In this work, we have obtained highly analogous results for AEI analogue, showing that it retained the inhibitory activities toward SGPB, but lost most of inhibitory activity toward PPE. It is worth noting here that the inhibitory specificity of AEI could be affected by a restricted region in comparison with P14C/N39C. In both cases, each N-terminal loop near the reactive site moves by 3.7−4.0 Å toward the central helix to form the introduced disulfide bond. Such a conformational change would lead to loss of inhibitory activity toward PPE. Further, in the ^{15}N HSQC spectra, we observed the resonance signals for Cys^6, Ile^7, and Cys^8 in AEI analogue at 25 °C (Figure S3 of the Supporting Information). Contrary to this, the resonance signals for Leu^6, Ile^7, and Cys^8 in the wild type were missing at 25 °C; those for Leu^6 and Ile^7 were observable as broad peaks at 40 °C, and that for Cys^8 was observed at 50 °C (see also Figure S3 of the Supporting Information). These results indicate that conformational exchange on time scales of milliseconds to microseconds occurring in the N-terminal loop region (Pro^5-Leu^6-Ile^7-Cys^8) of the wild type is suppressed in the analogue, while extensive relaxation analysis is necessary to provide information about its amplitude.

Next, we describe the inhibitory specificity change of AEI analogue based on the comparison with the complex structures of OMTKY3 bound to serine proteases, such as CHT, SGPB, and HLE, by X-ray crystallography (*60*−*62*). The general binding mode is that residues P_6-P_3' of the inhibitor, particularly the P_3-P_2' region as the canonical binding loop of the Kazal-type inhibitors, interact with subsites of the enzyme in an antiparallel β-sheet fashion with the intermolecular hydrogen bonds. We calculated the pairwise rmsd values of main chain atoms in the P_3-P_2' region between AEI (AEI analogue) and OMTKY3 bound to serine proteases. The calculated value was 1.02 Å between AEI and OMTKY3 in complex with HLE and 1.05 Å between AEI and OMTKY3 in complex with SGPB. The values for AEI analogue were 1.17 and 1.20 Å, respectively. These results reasonably assume that each conformation of the canonical binding loop of wild-type AEI (and of AEI analogue) should be similar to that of OMTKY3 bound to serine proteases.

To examine the complementarities between enzymes and AEI (or AEI analogue), we constructed the hypothetical complex between AEI (or AEI analogue) and PPE (or HLE or SGPB) in a simple model building experiment (*40*). Both hypothetical AEI−PPE and AEI analogue−PPE complexes have unfavorable close contacts between the N-terminal loop region (Pro^5 of AEI and Pro^5 and Ile^7 of AEI analogue) of the inhibitors and enzyme. From comparison of the ^{15}N HSQC spectra of AEI with those of AEI analogue, we found that the N-terminal loop region (Pro^5-Leu^6-Ile^7-Cys^8) of the wild type is more flexible than that of AEI analogue, as described above. It appeared, therefore, that wild-type AEI could change its conformation in that region to prevent the unfavorable close contacts with PPE, whereas AEI analogue could not, probably because of the reduced conformational plasticity of the region due to introduction of a Cys^6-Cys^{31} bond. Our results also assume that the hypothetical AEI analogue−SGPB complex has bad contacts even though AEI analogue strongly inhibits SGPB. Most of the structural differences between PPE and other serine proteases, such as SGPB, are located in surface loops (*63*). SGBP has a smaller surface loop, which would accommodate inhibitors more easily than PPE. Thus, the engineered disulfide bond might have little effect on the inhibitory activity of AEI analogue against SGBP.

Considering that the canonical binding loop of wild-type AEI (and of AEI-analogue) would be similar to that of OMTKY3 bound to serine proteases, it is tempting to speculate that the inhibitory specificity change of AEI analogue is due to the change in the steric conflict between inhibitor and enzyme but not the loss of the intermolecular hydrogen bonds between them. This provides a potential framework for further understanding the relationship between the inhibitory activity and the conformational flexibility of the Kazal-type inhibitors.

ACKNOWLEDGMENT

We thank Dr. Evelyn Stimson for her helpful discussions.

SUPPORTING INFORMATION AVAILABLE

Complete synthetic details and protein characterization details, one table containing amino acid compositions and molecular masses of AEIs and their thermolytic fragments, and three figures summarizing the sequential NOE connectivities (Figure S1), showing the backbone pairwise rmsd per residue between each minimized average structure of AEI and AEI analogue (Figure S2), and showing three ^{1}HN−^{15}N HSQC spectra of AEI or AEI analogue at 25 or 40 °C (Figure S3). This material is available free of charge via the Internet at http://pubs.acs.org.

REFERENCES

1. Kolkenbrock, H., and Tschesche, H. (1987) A new inhibitor of elastase from the sea anemone (*Anemonia sulcata*), *Biol. Chem. Hoppe-Seyler 368*, 93−99.
2. Tschesche, H., Kolkenbrock, H., and Bode, W. (1987) The covalent structure of the elastase inhibitor from *Anemonia sulcata*: A "non-classical" Kazal-type protein, *Biol. Chem. Hoppe-Seyler 368*, 1297−1304.
3. Bode, W., Epp, O., Huber, R., Laskowski, M., Jr., and Ardelt, W. (1985) The crystal and molecular structure of the third domain of silver pheasant ovomucoid (OMSVP3), *Eur. J. Biochem. 147*, 387−395.
4. Johansson, M. W., Keyser, P., and Soderhall, K. (1994) Purification and cDNA cloning of a four-domain Kazal proteinase inhibitor from crayfish blood cells, *Eur. J. Biochem. 223*, 389−394.
5. Odum, L., Bundgaard, J. R., and Johnsen, A. H. (1999) A Kazal-type trypsin inhibitor from the protochordate *Ciona intestinalis*, *Eur. J. Biochem. 259*, 872−876.
6. Tamaoki, H., Miura, R., Kusunoki, M., Kyogoku, Y., Kobayashi, Y., and Moroder, L. (1998) Folding motifs induced and stabilized by distinct cystine frameworks, *Protein Eng. 11*, 649−659.
7. Tamaoki, H., Kobayashi, Y., Nishimura, S., Ohkubo, T., Kyogoku, Y., Nakajima, K., Kumagaye, S., Kimura, T., and Sakakibara, S. (1991) Solution conformation of endothelin determined by means of ^{1}H NMR spectroscopy and distance geometry calculations, *Protein Eng. 4*, 509−518.
8. Kobayashi, Y., Sato, A., Takashima, H., Tamaoki, H., Nishimura, S., Kyogoku, Y., Ikenaka, K., Kondo, T., Mikoshiba, K., Hojo, H., Aimoto, S., and Moroder, L. (1991) A new α-helical motif in membrane active peptides, *Neurochem. Int. 18*, 525−534.
9. Kobayashi, Y., Takashima, H., Tamaoki, H., Kyogoku, Y., Lambert, P., Kuroda, H., Chino, N., Watanabe, T. X., Kimura, T., Sakakibara, S., and Moroder, L. (1991) The cystine stabilized α-helix. A common structural motif of ion channel blocking neurotoxic peptides, *Biopolymers 31*, 1213−1220.
10. Pease, J. H., and Wemmer, D. E. (1988) Solution structure of apamin determined by nuclear magnetic resonance and distance geometry, *Biochemistry 27*, 8491−8498.
11. Takashima, H., Kobayashi, Y., Tamaoki, H., Kyogoku, Y., Lambert, P., Kuroda, H., Chino, N., Watanabe, T. X., Kimura, T., and Sakakibara, S. (1991) Solution structure of charybdotoxin determined by NMR and distance geometry, in *Peptides 1990* (Giralt, E., and Andreu, D., Eds.) pp 557−559, ESCOM, Leiden, The Netherlands.
12. Bruix, M., Jimenez, M. A., Santoro, J., Gonzalez, C., Colilla, F. J., Mendez, E., and Rico, M. (1993) Solution structure of γ1-H and γ1-P thionins from barley and wheat endosperm determined by ^{1}H NMR: A structural motif common to toxic arthropod proteins, *Biochemistry 32*, 715−724.
13. Friedrich, T., Kroger, B., Bialojan, S., Lemaire, H. G., Hoffken, H. W., Reuscenbach, P., Otte, M., and Dodt, J. (1993) A Kazal-type inhibitor with thrombin specificity from *Rhodnius prolixus*, *J. Biol. Chem. 268*, 16216−16222.
14. Sommerhoff, C. P., Sollner, C., Mentele, R., Piechottka, G. P., Auerswald, E. A., and Fritz, H. (1994) A Kazal-type inhibitor of human mast cell tryptase: Isolation from the medical leech *Hirudo medicinalis*, characterization, and sequence analysis, *Biol. Chem. Hoppe-Seyler 375*, 685−694.
15. Hemmi, H., Yoshida, T., Kumazaki, T., Nemoto, N., Hasegawa, J., Nishioka, F., Kyogoku, Y., Yokosawa, H., and Kobayashi, Y. (2002) Solution structure of ascidian trypsin inhibitor determined by nuclear magnetic resonance spectroscopy, *Biochemistry 41*, 10657−10664.
16. Hemmi, H., Kumazaki, T., Yamazaki, T., Kojima, S., Yoshida, T., Kyogoku, Y., Katsu, M., Shinohara, F., Yokosawa, H., Miura, K., and Kobayashi, Y. (2003) Inhibitory specificity change of the ovomucoid third domain of the silver pheasant upon introduction of an engineered Cys^{14}-Cys^{39} bond, *Biochemistry 42*, 2524−2534.
17. Laskowski, M., Jr., Kato, I., Ardelt, W., Cook, J., Denton, A., Empie, M. W., Kohr, W. J., Park, S. J., Parks, K., Schatzley, B. L., Schoenberger, O. L., Tashiro, M., Vichot, G., Whatkey, H. F., Wieczorek, A., and Wieczorek, M. (1987) Ovomucoid third domains from 100 avian species: Isolation, sequences, and hypervariability of enzyme−inhibitor contact residues, *Biochemistry 26*, 202−221.
18. Dawson, P. E., Muir, T. W., Clark-Lewis, I., and Kent, S. B. (1994) Synthesis of proteins by native chemical ligation, *Science 266*, 776−779.
19. Narahashi, Y. (1970) Pronase, *Methods Enzymol. 19*, 651−664.
20. Bender, M. L., Begue-Canton, M. L., Blakeley, R. L., Brubacher, L. J., Feder, J., Gunter, C. R., Kezdy, F. J., Killheffer, J. V., Jr., Marshall, T. H., Miller, C. G., Roeske, R. W., and Stoops, J. K. (1966) The determination of the concentration of hydrolytic enzyme solutions: α-Chymotrypsin, trypsin, papain, elastase, subtilisin, and acetylcholinesterase, *J. Am. Chem. Soc. 88*, 5890−5913.
21. Chase, T., Jr., and Shaw, E. (1970) Titration of trypsin, plasmin, and thrombin with *p*-nitrophenyl *p*′-guanidinobenzoate HCl, *Methods Enzymol. 19*, 20−27.
22. Bieth, J. G. (1995) Theoretical and practical aspects of proteinase inhibition kinetics, *Methods Enzymol. 248*, 59−84.
23. Marion, D., and Wüthrich, K. (1983) Application of phase sensitive two-dimensional correlated spectroscopy (COSY) for measurements of ^{1}H−^{1}H spin−spin coupling constants in proteins, *Biochem. Biophys. Res. Commun. 113*, 967−974.
24. Marion, D., Ikura, M., Tschundin, R., and Bax, A. (1989) Rapid recording of 2D NMR spectra without phase cycling. Application to the study of hydrogen exchange in proteins, *J. Magn. Reson. 85*, 393−399.
25. Rance, M., Sorensen, O. W., Bodenhausen, G., Wagner, G., Ernst, R. R., and Wüthrich, K. (1983) Improved spectral resolution in COSY ^{1}H NMR spectra of proteins via double quantum filtering, *Biochem. Biophys. Res. Commun. 117*, 479−485.
26. Davis, D. G., and Bax, A. (1985) Assignment of complex proton NMR spectra via two-dimensional homonuclear Hartmann−Hahn spectroscopy, *J. Am. Chem. Soc. 107*, 2820−2821.
27. Kumar, A., Ernst, R. R., and Wüthrich, K. (1980) A two-dimensional nuclear Overhauser enhancement (2D NOE) experiment for the elucidation of complete proton−proton cross-relaxation networks in biological macromolecules, *Biochem. Biophys. Res. Commun. 95*, 1−6.
28. Griesinger, C., and Ernst, R. R. (1987) Frequency offset effects and their elimination in NMR rotating-frame cross-relaxation spectroscopy, *J. Magn. Reson. 75*, 261−271.
29. Griesinger, C., Sorensen, O. W., and Ernst, R. R. (1987) Practical aspects of the E.COSY technique. Measurement of scalar spin−spin coupling constants in peptides, *J. Magn. Reson. 75*, 474−492.
30. Piotto, M., Saudek, V., and Sklenar, V. (1992) Gradient-tailored excitation for single-quantum NMR spectroscopy of aqueous solutions. *J. Biomol. NMR 2*, 661−665.
31. Sklenar, V., Piotto, M., Leppik, R., and Saudek, V. (1993) Gradient-tailored water suppression for ^{1}H-^{15}N HSQC experiments optimized to retain full sensitivity, *J. Magn. Reson. 102*, 241−245.
32. Bodenhausen, G., and Ruben, D. J. (1980) Natural abundance nitrogen-15 NMR by enhanced heteronuclear spectroscopy, *Chem. Phys. Lett. 69*, 185−189.
33. Wüthrich, K., Billetter, M., and Braun, W. (1983) Pseudo-structures for the 20 common amino acids for use in studies of protein conformations by measurements of intramolecular proton−proton distance constraints with nuclear magnetic resonance, *J. Mol. Biol. 169*, 949−961.
34. Clore, G. M., Gronenborn, A. M., Nilges, M., and Ryan, C. A. (1987) Three-dimensional structure of potato carboxypeptidase

inhibitor in solution. A study using nuclear magnetic resonance, distance geometry, and restrained molecular dynamics, *Biochemistry 26*, 8012−8013.
35. Wagner, G., Braun, W., Havel, T. F., Schaumman, T., Go, N., and Wüthrich, K. (1987) Protein structures in solution by nuclear magnetic resonance and distance geometry. The polypeptide fold of the basic pancreatic trypsin inhibitor determined using two different algorithms, DISGEO and DISMAN, *J. Mol. Biol. 196*, 611−639.
36. Brünger, A. T. (1992) *X-PLOR. A system for X-ray crystallography and NMR*, Yale University Press, New Haven, CT.
37. Laskowski, R. A., Rullmann, J. A. C., MacArthur, M. W., Kaptein, R., and Thornton, J. M. (1996) AQUA and PROCHECK-NMR: Programs for checking the quality of protein structures solved by NMR, *J. Biomol. NMR 8*, 477−486.
38. Koradi, R., Billeter, M., and Wüthrich, K. (1996) MOLMOL: A program for display and analysis of macromolecular structures, *J. Mol. Graphics 14*, 51−55.
39. Kraulis, P. J. (1991) MOLSCRIPT: A program to produce both detailed and schematic plots of protein structures, *J. Appl. Crystallogr. 24*, 946−950.
40. Read, R. J., and James, M. N. G. (1986) Introduction to the protein inhibitors: X-ray crystallography, in *Protease inhibitors* (Barrett, A. J., and Salvesen, G., Eds.) pp 301−336, Elsevier, Amsterdam.
41. Baker, M. B., and Murphy, K. P. (1997) Dissecting the energetics of a protein−protein interaction: The binding of ovomucoid third domain to elastase, *J. Mol. Biol. 268*, 557−569.
42. Wade, J. D., Bedford, J., Sheppard, R. C., and Tregear, G. W. (1991) DBU as an N α-deprotecting reagent for the fluorenylmethoxycarbonyl group in continuous flow solid-phase peptide synthesis, *Pept. Res. 4*, 194−199.
43. Lauer, J. L., Fields, C. G., and Fields, G. B. (1995) Sequence dependence of aspartimide formation during 9-fluorenylmethoxycarbonyl solid-phase peptide synthesis, *Lett. Pept. Sci. 1*, 197−205.
44. Kumagaye, K. Y., Inui, T., Nakajima, K., and Sakakibara, S. (1991) Suppression of a side reaction associated with N^{im}-benzyloxymethyl group during synthesis of peptides containing cysteinyl residue at the N-terminus, *Pept. Res. 4*, 84−87.
45. Kumagaye, K. Y., Inui, T., Nakajima, K., Kimura, T., and Sakakibara, S. (1991) Side reaction during removal of N^{im}-benzyloxymethyl(Bom) group, *Pept. Chem. 4*, 61−66.
46. Empie, M. W., and Laskowski, M., Jr. (1982) Thermodynamics and kinetics of single residue replacements in avian ovomucoid third domains: Effect on inhibitor interactions with serine proteinases, *Biochemistry 21*, 2274−2284.
47. Wüthrich, K. (1986) *NMR of Proteins and Nucleic Acids*, John Wiley & Sons, New York.
48. Fink, E., Rehm, H., Gippner, C., Bode, W., Eulitz, M., Machleidt, W., and Fritz, H. (1986) The primary structure of bdellin B-3 from the leech *Hirudo medicinalis*. Bdellin B-3 is a compact proteinase inhibitor of a "non-classical" Kazal type. It is present in the leech in a high molecular mass form, *Biol. Chem. Hoppe-Seyler 367*, 1235−1242.
49. Mende, K., Petoukhova, O., Koulitchkova, V., Schaub, G. A., Lange, U., Kaufmann, R., and Nowak, G. (1999) Dipetalogastin, a potent thrombin inhibitor from the blood-sucking insect *Dipetalogaster maximus*: cDNA cloning, expression and characterization, *Eur. J. Biochem. 266*, 583−590.
50. Tsunemi, M., Kato, H., Nishiuchi, Y., Kumagaye, S., and Sakakibara, S. (1992) Synthesis and structure−activity relationships of elafin, an elastase-specific inhibitor, *Biochem. Biophys. Res. Commun. 185*, 967−973.
51. Tan, N. H., and Kaiser, E. T. (1976) Studies on the solid-phase synthesis of bovine pancreatic trypsin inhibitor (Kunitz) and the characterization of the synthetic material, *J. Org. Chem. 41*, 2787−2793.
52. De Filippis, V., Vindigni, A., Altichieri, L., and Fontana, A. (1995) Core domain of hirudin from the leech *Hirudinaria manillensis*: Chemical synthesis, purification, and characterization of a Trp3 analog of fragment 1−47, *Biochemistry 34*, 9552−9564.
53. Heinz, D. W., Hyberts, S. G., Peng, J. W., Priestle, J. P., Wagner, G., and Grutter, M. G. (1992) Changing the inhibitory specificity and function of the proteinase inhibitor eglin c by site-directed mutagenesis: Functional and structural investigation, *Biochemistry 31*, 8755−8766.
54. Kojima, S., Kumagai, I., and Miura, K. (1993) Requirement for a disulfide bridge near the reactive site of protease inhibitor SSI (*Streptomyces* subtilisin inhibitor) for its inhibitory action, *J. Mol. Biol. 230*, 395−399.
55. Kojima, S., Obata, S., Kumagai, I., and Miura, K. (1990) Alteration of the specificity of the *Streptomyces* subtilisin inhibitor by gene engineering, *Biotechnology 8*, 449−452.
56. Kowalski, D., Leary, T. R., McKee, R. E., Sealock, R. W., Wang, D., and Laskowski, M., Jr. (1974) Replacements, insertions, and modifications of amino acid residues in the reactive site of soybean trypsin inhibitor (Kunitz), in *Proceedings of Bayer Symposium, V. Protease Inhibitors* (Fritz, H., Tschesche, H., Greene, L. J., and Truscheit, E., Eds.) pp 311−324, Springer, Berlin.
57. Jallat, S., Carvallo, D., Tessier, L. H., Roecklin, D., Roitsch, C., Ogushi, F., Crystal, R. G., and Courtney, M. (1986) Altered specificities of genetically engineered α1 antitrypsin variants, *Protein Eng. 1*, 29−35.
58. von Wilcken-Bergmann, B., Tilis, D., Sartorius, J., Auerwald, E. A., Schroder, W., and Müller-Hill, B. (1986) A synthetic operon containing 14 bovine pancreatic trypsin inhibitor genes is expressed in *E. coli*, *EMBO J. 5*, 3219−3225.
59. Longstaff, C., Campbell, A. F., and Fersht, A. R. (1990) Recombinant chymotrypsin inhibitor 2: Expression, kinetic analysis of inhibition with α-chymotrypsin and wild-type and mutant subtilisin BPN′, and protein engineering to investigate inhibitory specificity and mechanism, *Biochemistry 29*, 7339−7347.
60. Bode, W., Wei, A.-Z., Huber, R., Meyer, E., Travis, J., and Neumann, S. (1986) X-ray structure of the complex of human leukocyte elastase (PMN elastase) and the third domain of the turkey ovomucoid inhibitor, *EMBO J. 5*, 2453−2458.
61. Read, R. J., Fujinaga, M., Sielecki, A. R., and James, M. N. G. (1983) Structure of the complex of *Streptomyces griseus* protease B and the third domain of the turkey ovomucoid inhibitor at 1.8-Å resolution, *Biochemistry 22*, 4420−4433.
62. Fujinaga, M., Sielecki, A. R., Read, R. J., Ardelt, W., Laskowski, M., Jr., and James, M. N. G. (1987) Crystal and molecular structures of the complex of α-chymotrypsin with its inhibitor turkey ovomucoid third domain at 1.8 Å resolution, *J. Mol. Biol. 195*, 397−418.
63. Bode, W., Meyer, E., Jr., and Powers, J. C. (1989) Human leukocyte and porcine pancreatic elastase: X-ray crystal structures, mechanism, substrate specificity, and mechanism-based inhibitors, *Biochemistry 28*, 1951−1963.

BI0472806